This is a preprint, the final version is subject to change, of the American Mineralogist (MSA)
Cite as Authors (Year) Title. American Mineralogist, in press.
(DOI will not work until issue is live.) DOI: http://dx.doi.org/10.2138/am-2015-4859

Revision 2:

In-situ measurements of fluorine and chlorine speciation and partitioning between melts and aqueous fluids in the Na_2O-Al_2O_3-SiO_2-H_2O system

Celia Dalou *, Bjorn O. Mysen and Dionysis Foustoukos

Carnegie Institution of Washington

5241 Broad Branch Rd, NW

Washington DC

*Now at:

Department of Geological Sciences, Jackson School of Geosciences

The University of Texas at Austin

1 University Station C1100, Austin, TX 78712

ABSTRACT

The effect of pressure and temperature on the structure of silicate melts coexisting with silica-saturated aqueous electrolyte fluids enriched in fluorine or chlorine in the Na_2O–Al_2O_3–SiO_2–H_2O system has been described. In-situ measurements were conducted with the samples at desired temperatures and pressures in a hydrothermal diamond anvil cell (HDAC) by using microRaman and FTIR spectroscopy techniques. The data were acquired at temperatures and pressures up to 800ºC and 1264 MPa, respectively.

In silicate melts, the intensity of the infrared bands assigned to the stretch

vibration of OH-groups is smaller than those of coexisting molecular H_2O when F and Cl are present in the melt structure. This difference reflects the interaction of F or Cl with H_2O in the melts. With decreasing pressure and temperature (*P-T)* conditions, SiF complexes are favored in the melt over that in coexisting fluid, perhaps because of decreasing silicate concentration in fluids with decreasing temperature and pressure. In these melts, the solubility of Cl, likely in the form of NaCl, increases with decreasing *P-T* conditions, whereas the abundance of such complexes in coexisting fluids decreases in favor of HCl.

Our experimental data were employed to model the ascent of a fluid-saturated magma from the upper mantle to the shallow crust. This modeling offers insights into F and Cl partitioning between and the speciation of F and Cl in melts and magmatic fluids. We suggest that the formation of stable SiF and NaCl complexes and their increasing solubilities in silicate melts during magma ascent may explain the late volcanic degassing of F and Cl compared with the degassing behavior of other volatile species.

Keywords: Fluorine, chlorine, speciation, aqueous fluids, hydrous melts, structure, spectroscopy, hydrothermal diamond anvil cell.

INTRODUCTION

Characterization of the behavior of volatile elements during magma ascent is central to constraining the cycling of volatiles from the Earth's interior to the surface. Volatile species are released into the atmosphere mainly through magma degassing and their abundance in the emitted gases and fluids is controlled by their speciation and solubility in melts and magmatic fluids.

Previous studies have focused on the characterization of volatile species (H_2O, CO_2, S, Cl and F) and their solubility in magmas of various compositions (e.g., Mysen et al. 1975; Mysen 1977; Eggler et al. 1979; Dixon et al. 1995; Webster et al. 1999; Brooker et al. 2001; Tamic et al. 2001; King and Holloway 2002; Signorelli and Carroll 2002; Botcharnikov et al. 2004). The solubility of volatile halogens and the depth of their exsolution depend on not only on magma composition but also on the concentration of other volatiles, especially H_2O and CO_2, which affects the solubility and fractionation of halogen-bearing species in and between minerals, melts and fluids (e.g., Holloway 1976; Carroll and Webster 1994; Dixon et al. 1995; Burgisser et al. 2008; Dalou and Mysen 2013). The partitioning of F and Cl between fluid and melt has been of special interest because these volatiles tend to degas during the latest stages of magmatic evolution (Carroll and Webster 1994; Spilliaert et al. 2006). While both F and Cl solubility in magmas can be quite high, their behavior in magmatic systems differs. For example, it is often concluded that Cl is dissolved preferentially in aqueous fluids, whereas F favors melts (Carroll and Webster 1994). However, comparative studies of F and Cl partitioning between fluid and melt with similar melt compositions, temperatures and pressures are rare as are data on degassing in volcanic systems (e.g. Pennisi and Le Cloarec 1998;

65 Spilliaert et al. 2006).

66 Earlier experiments measured species concentrations in quenched glasses and
67 calculated the composition of coexisting fluid after equilibration at high temperature and
68 pressure (Webster 1992; Métrich and Rutherford 1992, Lowenstern 1994; Shinohara
69 1994; Webster 1997; Signorelli and Carroll 2000; Chevychelov et al. 2008; Alleti et al.
70 2009). However, the structure of a silicate glass is different from that of its high-
71 temperature melt (e.g., Moynihan et al. 1976; Dingwell and Webb 1990), because silicate
72 speciation in the melt/glass structure is temperature (and pressure) dependent (e.g. Mysen
73 et al. 2003). Furthermore, the speciation of volatiles dissolved in melt is temperature-
74 dependent as observed, for instance, in the OH/H_2O (e.g., Nowak and Behrens 1995;
75 Sowerby and Keppler 1999) and CO_3/CO_2 ratios (Nowak et al., 2003). The speciation of
76 volatiles in fluid also changes with pressure and temperature, affecting estimates of
77 elemental solubility and speciation, for example those of C-O-H-N volatile components
78 (e.g. Mysen and Yamashita 2010; Mysen 2013a).

79 To circumvent barriers raised by examining melts and fluids quenched to ambient
80 pressure and temperature conditions, the *in-situ* experimental characterization of the melt
81 and fluid structure and composition at high pressure and high temperature is key.
82 Recently, experimental protocols employed have involved the integration of
83 hydrothermal diamond anvil cell (HDAC) techniques (e.g., Bassett et al. 1994; 1996)
84 with in-situ Raman and infrared spectroscopy (Shen and Keppler 1995; Nowak and
85 Behrens 1995; Zotov and Keppler 2000; 2002; Mysen 2010, 2011, 2012, 2013a). In this
86 paper, we present a series of HDAC experiments where such protocols are used to
87 constrain the effect of cooling and associated decompression on the Cl and F speciation

of a SiO_2-rich aqueous fluid and a coexisting H_2O-rich aluminosilicate melt. The experiments were conducted at upper mantle/deep crustal pressure and temperature conditions.

EXPERIMENTAL METHODS

A $Si_8AlNa_6O_{20}$ (NS3A5: 65wt% SiO_2, 7.8wt% Al_2O_3 and 28wt% Na_2O) composition glass was the silicate starting material (see Dalou et al. in review for analytical details of the glass). The glass was prepared by mixing spectroscopically pure Na_2CO_3, SiO_2 and Al_2O_3 powders, which were then decarbonated by slow step heating (50 ºC/15 minutes), and then melted for 2 hours at 1000 ºC. The aqueous fluids were pure deionized H_2O, 0.5 M of NaF and 0.5 M of NaCl.

The experiments were conducted with the samples in an externally heated hydrothermal diamond anvil cell (HDAC; Bassett et al. 1994, 1996) with 1 mm diamond culets. Samples comprised a small piece of NS3A5 glass, a small chip of synthetic ^{13}C diamond, and a < 1 µl drop of H_2O (Fig. 1 and 2). Reactants were contained in a 500 µm central hole of a 125 µm thick iridium gasket. The temperature in the HDAC was controlled to within 1 ºC with chromel-alumel thermocouples in contact with the surface of the upper and lower diamond anvils, however the accuracy of the temperature measurements is less than 3ºC (Bassett et al., 2000). The pressure was calculated from the pressure-/temperature-dependent one-phonon Raman shift of diamond (Bassett et al. 1996; Hanfland et al. 1985). To distinguish this shift from the Raman spectra of diamond anvils, we used synthetic ^{13}C diamond. Because of the mass difference between ^{12}C and ^{13}C diamonds (mass ratio, $\sqrt{m_{12C}/m_{13C}}$), their frequency difference is about 80 cm^{-1} at

ambient pressure and temperature (*P-T*) conditions but changes with *P-T* (Table 1, Fig. 3a). The one phonon Raman shift of ^{13}C diamond was calibrated in the 0.1 - 1300 MPa and 25° - 800 °C ranges, as described in Mysen and Yamashita (2010).

Raman spectra were obtained with a JASCO model IRS-3100 confocal microRaman spectrometer with holographic gratings. A 50X objective lens was employed for both visual microscopic examination and spectroscopic analysis. Signals were detected with an Andor Model DV401-F1 1024x128 pixel Peltier-cooled CCD (25 μm^2 pixels). To record spectra of melt and fluid, the 490.2 nm line of a solid-state laser was used. This laser operates at 33.3 mW on the sample. In these measurements, acquisition was performed with grating settings of 600 grooves/mm to cover the 178-4469 cm^{-1} frequency range within a single CCD window. The frequency resolution was ± 3 cm^{-1}. Acquisition time was typically 4 min per spectrum.

Spectra used to monitor pressure from the Raman shift of ^{13}C diamond were acquired with 2400 grooves/mm to cover the 1218–1753 cm^{-1} frequency range (covering the ^{12}C and ^{13}C diamond peaks and a Neon reference line) within a single CCD window. Here, a 532 nm laser line was used for sample excitation, operating at about 6.4 mW. By optimizing spectrometer frequency resolution to the 584.72 nm Ne emission line, the pressure precision is ± 40 MPa (± 0.1 cm^{-1} uncertainty on the Raman shift, Fig. 3). This precision combined with the uncertainty in the pressure calibration of the one-phonon shift of the ^{13}C diamond (±100 MPa; Mysen and Yamashita, 2010) yields a pressure uncertainty of about ±110 MPa.

Baseline correction of Raman spectra was performed on the JASCO® package spectra analysis software, as illustrated in Mysen et al. (2013). Curve-fitting of Raman

spectra was carried out using the IGOR™ software package from Wavemetrics™. In this procedure, location (Raman shift), bandwidth, and band intensity were treated as independent variables and minimization of χ^2 was used as the convergence criterion. Bandwidths were first fixed, and the number of bands and their locations were chosen according to Mysen et al. (2003) for NS3A5 composition melt and according to Mysen et al. (2010b) for fluids. Location and bandwidth were then restricted to vary within 40 cm^{-1} with minimization of χ^2 as the convergence criterion.

We also investigated the speciation of H_2O dissolved in the silicate melts by Fourier transform infrared spectroscopy (FTIR). Measurements were performed with a Jasco model IMV4000 FTIR microscope system with 10X objective and condenser cassegraine lenses, an InSb detector, CaF_2 beam splitter, and a halogen light source. Sixteen cm^{-1} resolution scans over the 750-7800 cm^{-1} frequency range were accumulated over 2048 scans when the aperture was ≥50x50 μm, and 4096 scans when smaller aperture was used.

In the halogen-free experiment, the size of each phase (melt globule, aqueous fluid) was smaller than the distance between diamond culets. Under such circumstances, the transmitted infrared signal at the point of interest will include contributions from both phases, and thus introduce interferences (Mysen, 2011). Therefore, no FTIR data on halogen-free fluids or melts are presented. Fluid or melt small volumes (<25x25 μm) in this experiment, however, were suitable for Raman spectroscopic measurements, which exploit a 1μm diameter laser beam and a focal depth near 10 μm. The F- and Cl-bearing aqueous fluids and melts were analyzed with both Raman and FTIR spectroscopy.

157 **Procedure**

158 These experiments describe melt and fluid equilibrium relationships at 800ºC. For
159 silicate glasses to melt and not dissolve into the fluid at this temperature, the density of a
160 coexisting fluid at *P-T* conditions needs to be sufficiently low so that fluid and melt can
161 coexist (Mysen 2013b) (Table 1). Control of the fluid density is accomplished by
162 bleeding air into the sample chamber during several heating-cooling stages. The final
163 experiment, analyzed by Raman and FTIR spectroscopy, is performed once the right
164 proportion of solid-fluid and gas are reached (Fig. 2, photomicrograph 1).

165 Iridium gaskets tend to deform at high *P-T* conditions (Fig. 2). Phase segregation
166 occurs, therefore, at slightly different *P-T* conditions during each cooling process because
167 of the variable internal volume between experiments (Table 1). The homogenization
168 temperatures reported in Table 1 reflect the point of gas-fluid separation during cooling.
169 Experimental *P-T* conditions (shown in Fig. 3b) and observed phases are summarized in
170 Table 1.

171

172 **RESULTS**

173 **Raman spectroscopy**

174 The 3000-4000 cm^{-1} and 700-1200 cm^{-1} frequency ranges (Fig 4A) include Raman bands
175 changing with *P-T* conditions (Fig. 4B and C) and the presence of Cl and F in both melt
176 and fluid. Therefore, these frequency ranges appear to be relevant to the characterization
177 of the structural roles of Cl and F in coexisting fluid and melt

178 **3000-4000 cm^{-1} frequency range.** This frequency range is dominated by an
179 asymmetric envelope with an intensity maximum near 3540 cm^{-1} together with a tail that

extends to lower frequencies. The low-frequency component of this intensity envelope is considered to reflect hydrogen bonding between the O-H groups in the melt and fluid phase (e.g., Ratcliffe and Irish 1982; Walrafen et al. 1986; Frantz et al. 1993; Kawamoto et al. 2004; Mysen and Yamashita 2010; Mysen 2013a). With increasing temperature, the band becomes more symmetric (Fig. 4) as the role of hydrogen bonding becomes less important with increasing temperature (Walrafen et al., 1986; Frantz et al., 1993). At any given temperature, the band is sharper in the fluid than in melt phase (Fig. 4).

700-1200 cm^{-1} frequency range. This frequency range provides structural information relevant to the aluminosilicate species referred to as Q-species, in melts and silicate-saturated fluids (e.g., Brawer and White 1975; Furukawa et al. 1981; McMillan 1984; Maekawa and Yokokawa 1997; Zotov and Keppler 1998; Mysen et al. 2003 or Mysen 2012 for review). There are two maxima in this frequency range: one between 700 and 800 cm^{-1} and one between 1000 and 1100 cm^{-1} (Fig. 4). The latter is more intense in the melt, whereas the maximum at 700-800 cm^{-1} is more prominent in fluids. Moreover, the integrated area of the 700-800 cm^{-1} region in the spectra of aqueous fluid decreases with increasing *P*-*T*, whereas it increases in the spectra of melt. The Raman band assigned to the Si-F stretching also resides in this frequency range near 990 cm^{-1} (Dalou and Mysen 2013).

Infrared spectroscopy

In the 4000-8000 cm^{-1} portion of the IR spectrum, there could be three bands near 4500, 5200 and 7200 cm^{-1} present in FTIR spectra of both H_2O-rich melt and silicate-rich fluid (Mysen 2009; 2011). In this study, the 4500 cm^{-1} band could not be discerned in the fluid

spectra. Furthermore, because we cannot unambiguously assess the extent of signal interferences by fluid in the melt IR spectra because the melt globules often do not fill entirely the volume between the two diamonds, these bands are treated qualitatively only. In detail, the ratio of the integrated area of the 4500 and 5200 cm^{-1} bands (A_{4500}/A_{5200}) in spectra of melt increases with increasing *P-T* conditions (Fig. 5). The dependence of the A_{4500}/A_{5200} ratio on temperature is lower in F- and Cl- bearing melts than in melts of the Na_2O-SiO_2-H_2O (Mysen 2009) and Na_2O-Al_2O_3-SiO_2-H_2O systems (Mysen 2011) (Fig. 5b). This could be because of possible interference of aqueous fluid on the spectra of melt (no OH-signal detected in spectra of fluids). Alternatively, the *P-T* paths in the experiments in the Na_2O-SiO_2-H_2O (Mysen 2009) and Na_2O-Al_2O_3-SiO_2-H_2O system (Mysen 2011) are different from those in the present experiments. These differences notwithstanding, the evolution of the A_{4500}/A_{5200} ratio with temperature is similar in the Na_2O-Al_2O_3-SiO_2-H_2O-F and Na_2O-Al_2O_3-SiO_2-H_2O-Cl systems. The temperature-dependent A_{4500}/A_{5200} ratios, whether in halogen-bearing or halogen-free systems (Mysen 2009, 2011) are comparable, even though the experiments were carried out along quite different pressure paths (Fig. 2b). This leads to the suggestion that pressure is not the main control on the A_{4500}/A_{5200} ratio.

The 4500 cm^{-1} and 5200 cm^{-1} bands often are used to identify structurally bonded OH groups and molecular H_2O, respectively, in aluminosilicate melts (Scholze 1956; Bartholomew and Schreurs 1980; Withers et al. 1999; Malfait 2009). Although the A_{4500}/A_{5200} ratio cannot be used to extract abundance of water species and total water content in these melts, because of the possible interference from fluid and insufficient information on molar absorption coefficients, it is worth noticing that the ratio of the

integrated peak areas of OH and H_2O increases with increasing temperature. In general, this ratio is lower in the halogen-bearing melt relative to the halogen-free aluminosilicate melt.

DISCUSSION

The structure of the melt and fluid phase

O-H bonding environment in aluminosilicate melts and aqueous fluids

The 3000-4000 cm^{-1} frequency envelope is assigned to OH stretch vibrations (e.g., Van Thiel et al. 1957; Velde 1983; McMillan and Remmele 1986; Frantz et al. 1993; Kawamoto et al. 2004; Mysen, 2011). Two Gaussian bands were fitted with one centered near 3530 cm^{-1} and the other near 3450 cm^{-1} (Fig. 6a); assigned to isolated and hydrogen-bonded OH groups, respectively (Foustoukos and Mysen 2012). The relative distribution of the integrated peak areas is used to constrain the stability of the O…H-O bonding in the H_2O component of the melt and fluid phase (Walrafen 1968; Walrafen et al. 1996). By assuming that the relative normalized differential Raman scattering cross sections (σ_j) of the O-H and O…H-O ν_1 vibrations are the same, the mole fraction ratio of isolated and hydrogen-bonded OH groups, X^{HYDR}/X^{ISOL}, equals the integrated intensities ratio:

$$K^{ISOL/HYDR} = X^{HYDR}/X^{ISOL} = A^{HYDR}/A^{ISOL} \quad (1)$$

From the correlation of $K^{ISOL/HYDR}$ with $1/T.10^3$, we estimate the enthalpy of rupture (ΔH) of the O…H-O intermolecular bond in aqueous fluids and H_2O-rich melts (Fig. 5; Walrafen 1968; Foustoukos and Mysen 2012). In halogen-free fluids, ΔH of 18 kJ/mol for hydrogen-bond formation was estimated, consistent with the value reported for

supercritical H_2O solution (21±1 kJ/mol) (Foustoukos and Mysen 2012). As observed in Mysen (2013a), the ΔH is significantly weaker in melts than in fluids: 10±2 kJ/mol in Na_2O-SiO_2-H_2O melts and 11 kJ/mol in Na_2O-Al_2O_3-SiO_2-H_2O melts. Note that the ΔH reported in Mysen (2013a) and this study are similar (within the error bar) even though they are from different pressures (to 800ºC - 1250 MPa and to 800ºC - 829 MPa, respectively). This suggests that pressure is not an important factor controlling ΔH. The reason for this difference remains unclear, but an initial hypothesis suggests that molecular H_2O might be partly isolated in cavities in the silicate melt structure (Mysen 2013a). Notably, the ΔH values for the hydrogen bonding in the halogen-free aqueous phase (Fig. 6b) are lower than those calculated for the Na_2O-Al_2O_3-SiO_2-H_2O-Cl system (Fig. 6d), but higher than the estimations in the Na_2O-Al_2O_3-SiO_2-H_2O-F system (Fig. 6c).

In short, the relative stability of the intermolecular hydrogen bond between OH groups in both melt and fluid can be expressed as $\Delta H_{Cl} > \Delta H_O > \Delta H_F$. While hydrogen bonding typically occurs where the partially positively charged hydrogen atom lies between partially negatively charged oxygen atoms, it has been shown experimentally at temperature up to 500ºC and pressure up to 500 MPa (Mayanovic et al. 2001) that hydrogen can form bonds with F^-, Cl^- (and Br^-) in fluids, such as HO-H$\cdots$$F^-$ and HO-H$\cdots$$Cl^-$ (see Collins et al. 2007 for review). The strength of hydrogen bonding is reduced as the halide radius increases (Collins et al. 2007). Statistical mechanics models have also suggested that charge densities control the ion-water interaction by affecting the two competing forces of electrostatic interaction (water's dipole interacting with ions) and the hydrogen bonding (water interacting with neighboring waters) in water structure (Hribar

et al. 2002). Based on this model, small ions (e.g. F^-) exhibit large charge densities that cause strong electrostatic ordering within water molecules and disrupt the water-water hydrogen bonds in the first solvation shell. To this end, the HO-H$\cdots F^-$ bond appears to be weak (ΔH-value: 2.2 kJ/mol at temperatures ranging from 300 to 800ºC and pressures between 143 to 606 MPa, Table 1). In contrast, the HO-H$\cdots Cl^-$ bond is stronger in fluid (ΔH-value: 37.5 kJ/mol; at 300 to 800 ºC and between 246 to 1264 MPa, Table 1) than the hydrogen bond in water HO-H$\cdots OH_2$ at high P-T (ΔH-value: 21±1 kJ/mol, at 300-800 ºC, 330-1340 MPa, Foustoukos and Mysen 2012). This is consistent with Bondarenko et al. (2006) who show that at 100 MPa, <500ºC in the H_2O-NaCl system the Cl$\cdots$H electrostatic attraction is stronger than O$\cdots$H bonds between H_2O molecules (O_{H_2O} partial charge is $-0.82|e|$ in the SPC water model, while Cl^-_{H2O} full formal charge is $-1|e|$).

In the case of the melt phase, charge density differences appear to impose less of an effect on the stability of the hydrogen intermolecular bonds. For example, the ΔH-value of hydrogen bonding measured in F-bearing NS3A5 melts (3.1 kJ/mol; at 300 to 800ºC – 143 to 606MPa) compares well with C$\cdots$H-OH_2 (theoretically predicted ~ 4 kJ/mol; Li et al. 2007; Scheiner 2010), a structural behavior attributed to their comparable atomic radii, 0.072 and 0.077 nm, respectively.

The effect of fluorine and chlorine on the structure of H_2O-rich aluminosilicate melts

The 700-1200 cm^{-1} frequency range of Raman spectra is assigned to the stretch vibrations of Si-O and Al-O in aluminosilicate melts and fluids (see, for example, Mysen and Richet 2005), supported by ^{29}Si and ^{27}Al NMR spectroscopy in silicate glasses and

295 silicate-rich aqueous fluids (e.g. Stebbins 1987; Kinrade and Swaddle 1988; Buckermann
296 et al. 1992; Kinrade 1996; Mysen and Cody 2005; Mysen 2007; Mysen et al. 2011).

297 Examples of curve-fitting results, deconvolved following Gaussian distributions,
298 from the 700-1200 cm^{-1} frequency range are presented in Figure 7. There are 4 main
299 bands near 750-820, 820-860, 870-910 and 1070-1090 cm^{-1} associated with
300 aluminosilicate structural units with 4, 3, 2 and 1 non-bridging atoms for the Q^0, Q^1, Q^2
301 and Q^3 structural units, respectively. A band around 1050 cm^{-1} is observed in all spectra
302 (Fig. 7). This band likely corresponds to (Si,Al)–O° vibrations in any structural units with
303 bridging oxygen (Mysen et al., 1982; Lasaga, 1982). However, its assignment is still
304 debatable (Mysen, 2007; Mysen and Cody, 2005) and will not be discussed any further.
305 Bandwidth and location of Q^n species' bands are constant among spectra (within 10 cm^{-1}
306 and 40 cm^{-1}, respectively).

307 By assuming that the ratio of Raman cross-sections for the Si-O vibrations of the
308 Q^0, Q^1, Q^2 and Q^3 are similar, the ratio of integrated intensities is the same as the ratio of
309 mole fractions (Mysen et al. 2013). The abundance of Q^n species in melts and fluids,
310 derived in this manner, are presented in Table 2. The location and bandwidth of the band
311 around 1050 cm^{-1} strongly depends on the noise in the 960-1000 cm^{-1} area, which can
312 reach up to 25% of the spectra intensity. Although the 1050 cm^{-1} band was not taken into
313 account in the calculation of Q^n species mole fraction, its area can induce an uncertainty,
314 in particular regarding Q^3 mole fraction. This uncertainty is difficult to estimate but we
315 consider that it cannot account for the whole variation of Q^n mole fractions derived from
316 the spectra (Figures 7 and 8).

317 Differences between the relative abundances of silicate species in the hydrous

318 melt and aqueous fluid are immediately evident (Fig. 7). The abundance of the more
319 polymerized species, Q^2 and Q^3, is greater in melts than in fluids, whereas the most
320 depolymerized species, Q^0, is found to be more abundant in fluids (Fig. 7). The most
321 polymerized Q^n species, Q^3, is less abundant in F- and Cl-bearing aqueous fluids than in
322 the halogen-free fluid (Table 2). This suggests that F and Cl presence in fluids disrupts
323 the fluid structure, perhaps by depolymerizing the silicate network. Our experimental
324 data suggest that such an effect might be greater in F-bearing relative to Cl-bearing
325 fluids.

326 From the integrated peak area of bands assigned to Si-O stretch vibrations in the
327 individual Q^n species normalized to the sum of all Q^n species areas, we calculated
328 fluid/melt partition coefficients, $D^{fluid/melt}$ (Fig. 8). The $D^{fluid/melt}$ of the most
329 depolymerized Q^n species, Q^0, decreases rapidly with increasing temperature, and
330 therefore pressure (as increasing temperature drives increased pressure, Fig. 3b), in all
331 experiments. In contrast, the partition coefficients of more polymerized species, Q^2 and
332 Q^3, increase with increasing temperature/-pressure in the halogen-free experiment (Fig.
333 8).

334 Interestingly, the dependence of Q^n abundance on *P-T* conditions is modified by
335 the presence of F and Cl in the system (Fig. 8). In the F-bearing system, with increasing
336 *P-T*, the partition coefficients of the most depolymerized species, Q^0, and Q^1 decrease
337 whereas that of the most polymerized species, Q^3, increases but remains lower than in the
338 halogen-free system. A small effect is observed in the case of the Cl-bearing system.
339 Moreover, $D^{fluid/melt}_{Q3}$ initially decreases from 400 to 600ºC and then increases at higher
340 temperature, ergo higher pressure. These trends tend to suggest that the depolymerization

effect of H_2O in highly alkaline aluminosilicate melts is less effective in the presence of Cl.

Fluorine speciation and fluid/melt partitioning

Curve fitting of the Raman spectra of F-bearing melts and fluids requires the presence of a band near 990 cm^{-1}. This is attributed to the Si-F in Q^3, noted $Q^3(F)$, assuming that the replacement of O^{2-} by F^- likely causes a reduced vibrational frequency and that the 990 cm^{-1} band is just lower than the frequency of Si-O vibrations in Q^3. Furthermore, this frequency is near the Si-F stretching vibration of SiO_3-F complexes (~ 945cm^{-1}; Dumas et al., 1982; Yamamoto et al., 1983) in silicate glasses.

The integrated area of the 990 cm^{-1} peak (normalized to the sum of all Q^n species areas) was used to calculate the partition coefficient of Si-F between fluids and melts, because the cross section for Si-F stretching is similar in fluids and melts assuming that the (Si+F)-species are the same in fluids and melts. With increasing *P-T* conditions, the $D^{fluid/melt}_{Si-F}$ increases (Fig. 9a). The linear regression of the relationship between $\ln(D^{fluid/melt}_{Si-F})$ and $1/T$, results in a ΔH = -15.2 ±0.6 kJ/mol (Fig. 9b) for the equilibrium exchange of Si-F between fluid and melt. This value is comparable to the ΔH we find for Q^3 *(*-16 ±2 kJ/mol, Fig. 9c), suggesting that F does not significantly disturb the silicate structure.

Water solubility in melts increases and progressively depolymerizes melts with increasing *P-T* in our *P-T* condition range (Table 2). During melt depolymerization, the relative abundance of Q^3 and, therefore, of $Q^3(F)$ decreases (Table 2), while there is no evidence of Si-F vibrations in more depolymerized species Q^2 or Q^1 (no shoulders on the

lower frequency parts of Q^2 or Q^1 bands are observed). Results, therefore, indicate that the Si-F concentration in melts decreases with increasing *P-T* (Table 2). In silicate–rich aqueous fluids at low *P-T* conditions (200-400 ºC and 50-150 MPa), F and OH complexes with Si may form SiF_4, SiF_5^-, SiF_6^{2-} $Si(OH)_2F_2$, $H_3SiO_4^-$ and H_4SiO_4 (Konyshev and Aksyuk 2008). Konyshev and Aksyuk (2008) observe that, with increasing *P-T*, the abundance of the F-bearing complexes in fluids increases, while the abundance of Si-OH complexes decreases. Consistently, we observe that the solubility of these Si-F complexes in the fluid phases increases with increasing *P-T* (Table 2), regardless of complex speciation.

As *P-T* increases, FTIR *in-situ* measurements indicate that the OH/H_2O proportion increases in melts (Figure 5b). The OH/H_2O ratio increase in the halogen-free systems is similar although the two sets of data in the NS4 (Mysen 2009) and NA10 (Mysen 2011) systems are from different pressures (up to 1033 and 791 MPa, respectively) than the present experiments. The OH/H_2O increase with temperature is smaller in F-bearing melts than halogen-free melts (Fig. 5b). This suggests that F suppresses the formation of OH bonds with silicate, which is consistent with the reaction, found in F-bearing hydrous glasses, quenched at 1400ºC – 1.5 GPa (Dalou and Mysen 2013):

$$2AlSi_2O_4F_3 + 2Q^3(OH) \leftrightarrow 3Q^3(F) + Q^4 + Q^2 + 2Al^{3+} + H_2O, \quad (2)$$

where $Q^3(OH)$ refers to Q^3 species with $2H^+$ per Si and $AlSi_2O_4F_3$ refers to a possible F-bearing aluminosilicate complex formed by F_2 solution mechanism in anhydrous glass (Dalou et al. in revision).

In effect, by forming Si-F bonds, F reduces the formation of Si-OH bonds in aluminosilicate melts and promotes the formation of molecular H_2O.

As shown in previous studies (Schaller et al. 1992; Mysen et al. 2004), F preferentially bonds with Al in some aluminosilicate glasses. The presence of F in four-fold and six-fold coordination around Al is recorded by the variation of Raman spectra intensity near 800 and 600 cm^{-1}, respectively. The resolution of our spectra in those frequencies is insufficient to resolve the variation of Al-F complexes. Therefore, changes of Al-F bonding with *P-T* conditions cannot be discussed in more detail.

Chlorine speciation and fluid/melt partitioning

Previous work on chloride solubility in melts and fluids has shown that it preferentially bonds with alkali network-modifiers (Ca, Na or K; e.g. Stebbins and Du, 2002; Sandland et al. 2004; Zimova and Webb 2006; Evans et al. 2008; Baasner et al. 2013). For example, Dalou and Mysen (2013), proposed that Cl dissolves in hydrous silicate melts following the equilibrium reaction:

$$2NaOH + Q^4 + Cl_2 \leftrightarrow 2NaCl + Q^2 + H_2O. \quad (3)$$

This reaction suggests that the formation of NaCl species in the melt structure releases molecular H_2O and implies that the presence of Cl reduces the formation of OH bonds with sodium. This likely explains the lower OH/H_2O ratio in Cl-bearing melts than in halogen-free melts (Fig. 4b). To this end, increased H_2O solubility in silicate melts along the *P-T* path shifts the equilibrium reaction (3) to the right.

It also has been proposed that Cl can be dissolved in melts as HCl, an abundant species in magmatic gases:

409 $$HCl_{fluid} + O^{2-}_{melt} \leftrightarrow Cl^{-}_{melt} + OH^{-}_{melt} \quad (4)$$

410 (Kogarko 1974; Burnham 1979). The Cl solubility, however, decreases as water content
411 increases in aluminosilicate melts (Dalou and Mysen 2013). Therefore, as *P*-*T* and H_2O
412 solubility increases in aluminosilicate melt, Cl and Na activity decreases. If HCl was the
413 dominant speciation of Cl in hydrous silicate melts, it would be expected than an H_2O
414 content increase in the melt would increase Cl solubility as:

415 $$2NaCl + H_2O \leftrightarrow 2HCl + Na_2O, \quad (5)$$

416 which is not observed in silicate melts. This would suggest that NaCl bonds in hydrous
417 aluminosilicate melts are more important than HCl.

418 Experimental data on the evolution of the HCl/NaCl ratio in melts and fluids have
419 been determined at lower pressure than in this study (below 150MPa) and with natural
420 composition melts (from basalt to rhyolite, e.g Williams et al. 1997; Shinohara, 2009). In
421 these experiments, it has been shown that the HCl/NaCl ratio increases with decreasing
422 Na/Al in silicate melts and with decreasing pressure (Shinohara 1987; Candela 1990).
423 Shinohara (2009) also illustrates that, below ~65MPa, HCl becomes more abundant than
424 NaCl in the aqueous fluid, regardless of the composition of the melt in equilibrium with
425 the fluid. In other words, the equilibrium reaction (5) shifts to the right (Sourirajan and
426 Kennedy 1962) probably because of the large difference in partial volumes of HCl and
427 NaCl in low-density phases at high temperature and low pressure conditions (Shinohara
428 and Fujimoto 1994). Therefore, we can assume that in the range of pressure studied here
429 (246-1264 MPa), the abundance of HCl in the melt, compared to NaCl, is too low to be
430 detected spectroscopically. Moreover, as pressure decrease, the HCl/NaCl increasingly
431 partitioned from the melt into the aqueous fluid (Williams et al. 1997). This implies that

HCl solubility increases more rapidly in fluids than in silicate melts during decompression.

Frank et al. (2003) found a positive correlation between the $NaCl_{fluid}/NaOH_{melt}$ ratio and the HCl concentration in the aqueous fluid. Their observation suggests exchange equilibrium of Cl between fluid and melt written as:

$$NaOH_{melt} + 2NaCl_{fluid} \leftrightarrow NaCl_{fluid} + HCl_{fluid} + Na_2O_{melt} \quad (6)$$

As pressure decreases, the equilibrium 6 is shifted to the right. This solution mechanism allows more Na^+ to be released in the melt as a network modifier. Because Na prefers to bond with non-bridging oxygen in Q^3 species, this likely explains the decrease of the abundance of Q^3 in the melt (Table 2) from 600ºC – 790 MPa to 400ºC – 358 MPa, and leads to the decreases of the $D^{fluid/melt}_{Q3}$ at low *P-T* (Fig. 8d). In summary, the Cl exchanges between melt and fluid, as pressure and temperature decrease, favors the formation of HCl and NaCl in fluids and reduces Cl solubility in melts. Nevertheless, this exchange reaction cannot be detected at elevated *P-T* conditions (> 600ºC – 790 MPa).

IMPLICATIONS

The cooling and decompression of NaF- and NaCl-bearing magmatic liquids in a chemically closed environment was considered to model the ascent of a magma-fluid system. Although this model is restricted to alkaline systems in the 143-1264 MPa pressure range (i.e. from upper mantle or deep crustal pressures (50 – 25 km) to shallow crustal depths (10 to 5 km)), it significantly contributes to explain why F and Cl are the last volatiles to be degassed by magmatic systems (Spilliaert et al. 2006). Our data on solubility, speciation and partitioning, during magma ascent and cooling can also explain

455 the difference in degassing between F and Cl.

456 Fluorine solubility during magma ascent is discussed using Si-F complex as a
457 proxy since we found no evidence of $HF_{(aq)}$ (weak bonds in fluids), while dissolved
458 $NaF_{(aq)}$ species are in trace amounts in aqueous fluids (Weber et al. 2000) and in
459 depolymerized melts (Mysen and Virgo, 1985). The positive correlation of $D^{fluid/melt}_{Si\text{-}F}$
460 with temperature (Fig 9a) suggests that during cooling and ascension, (Si-F) complexes
461 increasingly partitions from the fluid into the melt. This is consistent with the decreasing
462 solubility of Si-F complexes like $Si(OH)_2F_{2(aq)}$ observed in low pressure and temperature
463 fluids (50 -150 MPa and 200 – 400ºC) as the solubility of quartz decreases (Konyshev
464 and Aksyuk, 2008). The solubility of (Si-F) complexes increases in melt with decreasing
465 pressure and temperature (Fig. 9d), i.e. as the magma cools and ascents. Below 600ºC and
466 790 MPa, Si-F partition coefficients between melt and fluid becomes >1, e.g. Si-F
467 becomes more concentrated in melts than in fluids. Our data supports the enrichment of
468 fluorine in the melt during ascent and cooling continues even after exsolution of the fluid
469 phase from the magmatic liquid at the late stages of magmatic history.

470 The Cl-bearing magma-fluid system is characterized by the high solubility of
471 NaCl-bearing complexes in fluids. Such fluids or brines transported in the crust by
472 various volcanic systems can be observed in inclusions either as fluid inclusions trapped
473 in host crystals or in silicate melt inclusions (e.g. Lowenstern 1994; Zajacz et al. 2008),
474 or as part of hydrothermal systems in high-temperature reservoirs (e.g. Hedenquist and
475 Lowenstern 1994; Chiodini et al. 2001). The Cl solution mechanism in hydrous
476 aluminosilicate melts suggests that Cl solubility in melts increases during magma ascent,
477 as H_2O solubility decreases in the form of NaCl-melt complexes (Dalou and Mysen

2012) at pressures < 790 MPa. The exchange reaction (6) suggests that the NaCl concentration in melts starts to decrease, forming dissolved HCl in fluid at conditions below 600ºC – 790 MPa, During shallower decompression, the abundance of HCl may also become significant and, perhaps, exceed that of NaCl at shallow crustal pressures (< 65MPa, Shinohara 2009) particularly in fluids. Once saline fluids are separated from the magma to ascent in crustal veins, Cl degassing (i.e. HCl_{vapor}) from the residual magma is controlled by the extent of Cl solubility in melts determined by the magma composition, e.g. alkalinity (Frank 2003; Shinohara 2009). For instance, HCl solubility in basaltic melts is larger than in rhyolitic melts, while HCl exsolution from basalt occurs at lower pressure than from rhyolite (Shinohara 2009).

To this end, it appears that during ascent, F and Cl speciation favors their solution in melts (perhaps only up to 790 MPa for Cl). Therefore, their solubility remains high to shallow depth in the Earth, consistent with F and Cl being the last degassed volatiles from magmas (Spilliaert et al. 2006). We pose that such behavior explains why F and Cl are often undersaturated in magmas (Carroll and Webster 1994) and, therefore, do not degas significantly. As less than 15% of initial F content is degassed, Cl can be degassed to 50% of its initial content (Métrich and Wallace 2008), suggesting that F solubility in magmas remains higher than Cl likely due the increasing formation of HCl in the last ~ 5 - 25 km of decompression.

ACKNOWLEDGEMENTS

501 This research was conducted with support from NSF grant EAR-1212754 (BOM),
502 Dalou's Geophysical Lab Fellowship, NAI grant, NSF-EAR -1250499 to DIF. Careful
503 and constructive reviews of Drs. S. Penniston-Dorland, J. Webster and an anonymous
504 reviewer were greatly appreciated.
505

506 **REFERENCES**

507 Alletti, M., Baker, D. R., Scaillet, B., Aiuppa, A., Moretti, R., and Ottolini, L. (2009)
508 Chlorine partitioning between a basaltic melt and H_2O–CO_2 fluids at Mount Etna.
509 Chemical Geology, 263(1-4), 37–50. doi:10.1016/j.chemgeo.2009.04.003

510 Baasner, A., Schmidt, B.C. and Webb, S.L. (2013) Compositional dependence of the
511 rheology of halogen (F, Cl) bearing-aluminosilicate melts. Chemical Geology,
512 346(C), 172–183. doi:10.1016/j.chemgeo.2012.09.020

513 Bartholomew, R.F., and Schreurs, J. W.H. (1980) Wide-line NMR study of protons in
514 hydrosilicate glasses of different water content. Journal of Non-Crystalline
515 Solids, 38, 679-684.

516 Bassett, W.A., Shen A. H., Bucknum, M., and Chou, I. M. (1994) A new diamond cell
517 for hydrothermal studies to 2.5 GPa and from -190ºC to 1200ºC. Review of
518 Scientific Instruments. 64, 2340-2345.

519 Bassett, W.A., Wu, T. -C., Chou, I.-M., Haselton, T., Frantz, J. D., Mysen, B.O., Huang,
520 W.-L., Sharma, S.K. and Schiferl, D. (1996) The hydrothermal diamond anvil cell
521 (DAC) and its applications. In Mineral Spectroscopy: A Tribute to Roger G Burns
522 (eds. M. D. Dyar, C. A. McCammon and M. Schaefer). The Geochemical Society,
523 Houston.

524 Bassett, W.A., Anderson, A.J., Mayanovic, R.A., and Chou, I. (2000) Hydrothermal
525 diamond anvil cell for XAFS studies of first-row transition elements in aqueous
526 solution up to supercritical conditions. Chemical geology, 167(1), 3-10.

527 Bondarenko, G.V., Gorbaty, Y.E., Okhulkov, A.V., and Kalinichev, A.G. (2006)
528 Structure and hydrogen bonding in liquid and supercritical aqueous NaCl solutions

529 at a pressure of 1000 bar and temperatures up to 500ºC: A comprehensive
530 experimental and computational study. The Journal of Physical Chemistry
531 A, 110(11), 4042-4052.
532 Botcharnikov, R.E., Behrens, H., Holtz, F., Koepke, J. and Sato, H. (2004) Sulfur and
533 chlorine solubility in Mt. Unzen rhyodacitic melt at 850ºC and 200 MPa. Chemical
534 Geology, 213(1-3), 207-225.
535 Brawer, S.A. and White, W.B. (1975) Raman spectroscopic investigation of the structure
536 of silicate glasses. I. The binary alkali silicates. The Journal of Chemical Physics, 63,
537 2421.
538 Brooker, R.A., Kohn, S.C., Holloway, J.R. and McMillan, P.F. (2001) Structural controls
539 on the solubility of CO_2 in silicate melts. Part 1: bulk solubility data. Chemical
540 Geology, 174, 225-239.
541 Buckermann, W.-A., Muller-Warmuth, W., and Frischat, G.H. (1992) A further ^{29}Si
542 MAS NMR study on binary alkali silicate glasses. Glastechnische Berichte Glass
543 Science and Technology, 65, 18-21.
544 Burgisser, A., Scaillet, B., and Harshvardhan, (2008) Chemical patterns of erupting silicic
545 magmas and their influence on the amount of degassing during ascent. Journal of
546 Geophysical Research, 113(B12), B12204. doi:10.1029/2008JB005680
547 Burnham, C.W. (1979) Hydrothermal fluids at the magmatic stage. In: Barnes, H.L.
548 (Ed.), Geochemistry of Hydrothermal Ore Deposits. John Wiley & Sons, New York,
549 pp. 34-76.
550 Candela P.A. (1990) Theoretical constraints on the chemistry of the magmatic aqueous
551 phase. Special Paper 246, pp. 11–20. Geological Society of America.

552 Carroll, M.R., and Webster, J.D. (1994) Solubilities of sulfur, noble gases, nitrogen,
553 chlorine, and fluorine in magmas. Reviews in Mineralogy and Geochemistry, 30(1),
554 231-279.
555 Chevychelov, V.Y., Botcharnikov, R.E., and Holtz, F. (2008) Partitioning of Cl and F
556 between fluid and hydrous phonolitic melt of Mt. Vesuvius at ~850–1000 °C and
557 200 MPa. Chemical Geology, 256(3-4), 172–184.
558 Chiodini, G., Marini, L., and Russo, M. (2001) Geochemical evidence for the existence
559 of high-temperature hydrothermal brines at Vesuvio volcano, Italy. Geochimica et
560 Cosmochimica Acta, 65(13), 2129–2147.
561 Collins, K.D., Neilson, G.W. and Enderby, J.E. (2007) Ions in water: Characterizing the
562 forces that control chemical processes and biological structure. Biophysical
563 Chemistry, 128, 95-104.
564 Dalou, C., Mysen, B.O., and Cody, G.D. (2014) Solubility and solution mechanisms of
565 chlorine and fluorine in aluminosilicate melts at high pressure and high temperature**.**
566 *American Mineralogist,in revision.*
567 Dalou, C., and Mysen, B.O. (2013) The effect of water on fluorine and chlorine solubility
568 and solution mechanisms in aluminosilicate melts at high pressure and high
569 temperature. *IAVCEI, abstract 1A1_1A-O18*.
570 Dingwell, D.B., and Webb, S.L. (1990) Relaxation in silicate melts. European Journal of
571 Mineralogy, 2, 427–449.
572 Dixon, J.E., Stolper, E.M., and Holloway, J.R. (1995) An experimental study of water
573 and carbon dioxide solubilities in mid-ocean ridge basaltic liquids. Part I: Calibration
574 and solubility models. Journal of Petrology, 36(6), 1607–1631.

575 Dumas, P., Corset, J., Carvalho, W., Levy, Y., Neuman, Y. (1982) Fluorine-doped
576 vitreous silicate analysis of fiber optics preforms by vibrational spectroscopy.
577 Journal of Non-Crystalline Solids, 47, 239-242.
578 Eggler, D.H., Mysen, B.O., Hoering, T.C., and Holloway, J. R. (1979) The solubility of
579 carbon monoxide in silicate melts at high pressures and its effect on silicate phase
580 relations. Earth and Planetary Science Letters, 43, 321–330.
581 Evans, K.A., Mavrogenes, J.A., O'Neill, H.S., Keller, N.S., and Jang, L.Y. (2008) A
582 preliminary investigation of chlorine XANES in silicate glasses. Geochemistry
583 Geophysics Geosystems, 9, Q10003, doi:10.1029/2008GC002157.
584 Foustoukos, D., and Mysen, B.O. (2012) D/H isotopic fractionation in the H_2-H_2O system
585 at supercritical water conditions: Composition and hydrogen bonding effect.
586 Geochimica et Cosmochimica Acta, 86, 88–102.
587 Frank, M.R., Candela, P.A., and Piccoli, P.M. (2003) Alkali exchange equilibria between
588 a silicate melt and coexisting magmatic volatile phase: an experimental study at
589 800ºC and 100 MPa. Geochimica et Cosmochimica Acta, 67(7), 1415-1427.
590 Frantz, J.D., Dubessy, J., and Mysen, B.O. (1993) An optical cell for Raman
591 spectroscopic studies of supercritical fluids and its applications to the study of water
592 to 500ºC and 2000 bar. Chemical Geology, 106, 9–26.
593 Furukawa, T., Fox, K.E., and White, W.B. (1981) Raman spectroscopic investigation of
594 the structure of silicate glasses. III. Raman intensities and structural units in sodium
595 silicate glasses. Journal of Chemical Physics, 153, 3226–3237.
596 Hanfland, M., Syassen, K., Fahy, S., Louie, S.G., and Cohen, M.L. (1985) Pressure
597 dependence of the first-order Raman mode in diamond. Physical Review B, 31,

6896–6899.

Hedenquist, J.W., and Lowenstern, J.B. (1994) The role of magmas in the formation of hydrothermal ore deposits. Nature, 370, 519–527.

Holloway, J.R. (1976) Fluids in the evolution of granitic magmas: Consequences of finite CO_2 solubility. Geological Society of America Bulletin, 87, 1513–1518.

Hribar, B., Southall, N.T., Vlachy, V., and Dill, K.A. (2002) How ions affect the structure of water. Journal of the American Chemical Society, 124(41), 12302-12311.

Kawamoto, T., Ochiai, S., and Kagi, H. (2004) Changes in the structure of water deduced from the pressure dependence of the Raman OH frequency. Journal of Chemical Physics, 120, 5867–5870.

Kinrade, S.D. and Swaddle, T.W. (1988) Silicon-29 NMR studies of aqueous silicate solutions 1. Chemical shifts and equilibria. Inorganic Chemistry, 27, 4253–4259.

Kinrade, S.D. (1996) Oxygen-17 NMR study of aqueous potassium silicates. The Journal of Physical Chemistry, 100(12), 4760-4764.

King, P.L., and Holloway, J.R. (2002) CO_2 solubility and speciation in intermediate (andesitic) melts: the role of H_2O and composition. Geochimica et Cosmochimica Acta, 66(9), 1627–1640.

Kogarko, L.N. (1974) Role of volatiles. In: The Alkaline Rocks (H. Sorensen, ed.), pp 474-487, Wiley, London.

Konyshev, A.A., and Aksyuk, A.M. (2008) Experimentally determined quartz solubility in F-bearing aqueous fluids at 200–400 °C and 50–150 MPa and the calculation of the concentrations of possible silica species. Geochemistry International, 46(8), 826–

833. doi:10.1134/S0016702908080077

Lasaga A.C. (1982) Optimization of CNDO for molecular orbital calculation on silicates. Physics and Chemistry of Minerals 8, 36–46.

Li, Q., Wang, N. and Yu, Z. (2007) Effect of hydration on the C-H· · ·O hydrogen bond: A theoretical study, Journal of Molecular Structure: Theochem 847, 68-74.

Lowenstern, J.B. (1994) Chlorine, fluid immiscibility, and degassing in peraklaine magmas from Pantelleria, Italy. American Mineralogist, 79, 353–369.

Maekawa, H. and Yokokawa, T. (1997) Effects of temperature on silicate melt structure: A high temperature ^{29}Si NMR study of $Na_2Si_2O_5$. Geochimica et cosmochimica acta, 61(13), 2569-2575.

Malfait, W.J. (2009) The 4500 cm^{-1} infrared absorption band in hydrous aluminosilicate glasses is a combination band of the fundamental (Si, Al)-OH and OH vibrations. American Mineralogist, 94(5-6), 849-852.

Mayanovic, R.A, Anderson, A.J., Bassett, W.A., and Chou, I.-M. (2001) Hydrogen bond breaking in aqueous solutions near the critical point. Chemical Physics Letters, 336, 212-218.

McMillan, P.F. (1984) Structural studies of silicate glasses and melts-applications and limitations of Raman spectroscopy. American Mineralogist, 69, 622–644.

McMillan, P.F., and Remmele, R.L. (1986) Hydroxyl sites in SiO_2 glass: A note on infrared and Raman spectra. American Mineralogist, 71, 772–778.

Métrich, N., and Rutherford, M. (1992) Experimental study of chlorine behavior in hydrous silicic melts. Geochimica et Cosmochimica Acta, 56, 607–616.

Métrich, N., and Wallace, P.J. (2008) Volatile abundances in basaltic magmas and their

644 degassing paths tracked by melt inclusions. Reviews in Mineralogy and
645 Geochemistry, 69(1), 363–402. doi:10.2138/rmg.2008.69.10
646 Moynihan, C.T., Macedo, P.B., Montrose, C.J., Gupta, P.K., DeBolt, M.A., Dill, J.F., ...
647 and Wilder, J.A. (1976) Structural relaxation in vitreous materials. Annals of the
648 New York Academy of Sciences, 279(1), 15-35.
649 Mysen, B.O. (1977) The solubility of H_2O and CO_2 under predicted magma genesis
650 conditions and some petrological and geophysical implications. Reviews of
651 Geophysics and Space Physics, 15(3), 351–361.
652 Mysen, B. O., Finger, L. W., Virgo, D., and Seifert, F.A. (1982) Curve-fitting of Raman
653 spectra of silicate glasses. American Mineralogist, 67(7-8), 686-695.
654 Mysen, B.O. (2007) The solution behavior of H_2O in peralkaline aluminosilicate melts at
655 high pressure with implications for properties of hydrous melts. Geochimica et
656 Cosmochimica Acta, 71(7), 1820–1834. doi:10.1016/j.gca.2007.01.007
657 Mysen, B.O. (2009) Solution mechanisms of silicate in aqueous fluid and H_2O in
658 coexisting silicate melts determined *in-situ* at high pressure and high
659 temperature. Geochimica et Cosmochimica Acta, 73(19), 5748-5763.
660 Mysen, B. (2010a) Structure of H_2O-saturated peralkaline aluminosilicate melt and
661 coexisting aluminosilicate-saturated aqueous fluid determined *in-situ* to 800ºC and ~
662 800MPa. Geochimica et Cosmochimica Acta, 74(14), 4123-4139.
663 Mysen, B.O. (2010b) Speciation and mixing behavior of silica-saturated aqueous fluid at
664 high temperature and pressure. American Mineralogist, 95(11-12), 1807–1816.
665 doi:10.2138/am.2010.3539
666 Mysen, B.O. (2011) Amorphous Materials: An experimental study of phosphorous and

667 aluminosilicate speciation in and partitioning between aqueous fluids and silicate
668 melts determined in-situ at high temperature and pressure. American Mineralogist,
669 96(10), 1636–1649. doi:10.2138/am.2011.3728
670 Mysen, B.O. (2012) Silicate-COH melt and fluid structure, their physicochemical
671 properties, and partitioning of nominally refractory oxides between melts and fluids.
672 Lithos, 148(C), 228–246. doi:10.1016/j.lithos.2012.06.005
673 Mysen, B.O. (2013a) Structure–property relationships of COHN-saturated silicate melt
674 coexisting with COHN fluid: A review of *in-situ*, high-temperature, high-pressure
675 experiments. Chemical Geology, 346(C), 113–124.
676 Mysen, B. (2013b) Hydrogen isotope fractionation between coexisting hydrous melt and
677 silicate-saturated aqueous fluid: An experimental study in situ at high pressure and
678 temperature. American Mineralogist, 98(2-3), 376-386.
679 Mysen, B.O., and Cody, G.D. (2005) Solution mechanisms of H_2O in depolymerized
680 peralkaline melts. Geochimica et Cosmochimica Acta, 69(23), 5557–5566.
681 doi:10.1016/j.gca.2005.07.020
682 Mysen B.O., and Richet P. (2005) Silicate Glasses and Melts - Properties and Structure.
683 Elsevier, 548 pp.
684 Mysen, B.O., and Yamashita, S. (2010) Speciation of reduced C-O-H volatiles in
685 coexisting fluids and silicate melts determined in-situ to ~ 1.4 GPa and 800ºC.
686 Geochimica et Cosmochimica Acta, 74(15), 4577–4588.
687 Mysen, B.O., Arculus, R J., and Eggler, D.H. (1975) Solubility of carbon dioxide in melts
688 of andesite, tholeiite, and olivine nephelinite composition to 30 kbar pressure.
689 Contributions to Mineralogy and Petrology, 53, 227–239.

690 Mysen, B.O., Lucier, A., and Cody, G.D. (2003) The structural behavior of Al^{3+} in
691 peralkaline melts and glasses in the system Na_2O-Al_2O_3-SiO_2. American
692 Mineralogist, 88, 1668–1678.
693 Mysen, B.O., Cody, G.D., and Smith, A. (2004) Solubility mechanisms of fluorine in
694 peralkaline and meta-aluminous silicate glasses and in melts to magmatic
695 temperatures. Geochimica et Cosmochimica Acta, 68(12), 2745–2769.
696 Mysen, B.O., Kumamoto, K., Cody, G.D., and Fogel, M.L. (2011) Solubility and solution
697 mechanisms of C-O-H volatiles in silicate melt with variable redox conditions and
698 meltcomposition at upper mantle temperatures and pressures. Geochimica et
699 Cosmochimica Acta, 75(20), 6183–6199
700 Mysen, B.O., Mibe, K., Chou, I.M., and Bassett, W.A. (2013) Structure and equilibria
701 among silicate species in aqueous fluids in the upper mantle: Experimental SiO_2-
702 H_2O and MgO-SiO_2-H_2O data recorded in-situ to 900ºC and 5.4 GPa. Journal of
703 Geophysical Research: Solid Earth, 188, 6078-6085.
704 Nowak, M., and Behrens, H. (1995) The speciation of water in haplogranitic glasses and
705 melts determined by in-situ near-infrared spectroscopy. Geochimica et
706 Cosmochimica Acta, 59(16), 3445–3460.
707 Nowak, M., Porbatzki, D., Spickenbom, K. and Diedrich, O. (2003) Carbon dioxide
708 speciation in silicate melts: a restart. Earth and Planetary Science Letters 207, 131-
709 139.
710 Pennisi, M., and Le Cloarec, M.F. (1998) Variations of Cl, F and S in Mount Etna's
711 plume, Italy, between 1992 and 1995. Journal of Geophysical Research, 103(B3),
712 5061–5066.

713 Ratcliffe, C.I., and Irish, D.E. (1982) Vibrational studies of solutions at elevated
714 temperatures and pressures. 5. Raman studies of liquid water up to 300ºC. Journal of
715 Physical Chemistry, 86, 4897–4905.
716 Sandland, T.O., Du, L.-S., Stebbins, J.F., and Webster, J.D. (2004) Structure of Cl-
717 containing silicate and aluminosilicate glasses: A ^{35}Cl MAS-NMR study. Geochimica
718 et Cosmochimica Acta, 68(24), 5059–5069.
719 Schaller, T., Dingwell, D.B., Keppler, H., Knöller, W., Merwin, L., and Sebald, A.
720 (1992) Fluorine in silicate glasses: A multinuclear nuclear magnetic resonance study.
721 Geochimica et Cosmochimica Acta, 56, 701–707.
722 Scheiner S. (2010) Cooperativity of multiple H-bonds in influencing structural and
723 spectroscopic features of the peptide unit of proteins. Journal of Molecular
724 Structure, 976, 49-55.
725 Scholze, H. (1956) Der Einbau des Wassers in Glasern. 4th International Congress on
726 Glass, Paris, pp. 424–429.
727 Shen, A., and Keppler, H. (1995) Infrared spectroscopy of hydrous silicate melts to
728 1000ºC and 10 kbar: Direct observation of H_2O speciation in a diamond-anvil cell.
729 American Mineralogist, 80, 1335–1338.
730 Shinohara, H. (1987) Partition of chlorine compounds in the system silicate melt and
731 hydrothermal solutions. PhD Thesis, Tokyo Institute of Technology.
732 Shinohara, H. (1994) Exsolution of immiscible vapor and liquid phases from a
733 crystallizing silicate melt: Implications for chlorine and metal transport. Geochimica
734 et Cosmochimica Acta, 58(23), 5215–5221.

735 Shinohara, H. (2009) A missing link between volcanic degassing and experimental
736 studies on chloride partitioning. Chemical Geology, 263, 51-59.
737 Shinohara, H. and, Fujimoto, K. (1994) Experimental study in the system albite-
738 andalusite-quartz-NaCl-HCl-H_2O at 600ºC and 400 to 2000 bars. Geochimica and
739 Cosmochimica Acta, 58, 4857-4866.
740 Signorelli, S., and Carroll, M.R. (2000) Solubility and fluid-melt partitioning of Cl in
741 hydrous phonolitic melts. Geochimica et Cosmochimica Acta, 64(16), 2851–2862.
742 Signorelli, S., and Carroll, M.R. (2002) Experimental study of Cl solubility in hydrous
743 alkaline melts: constraints on the theoretical maximum amount of Cl in trachytic and
744 phonolitic melts. Contributions to Mineralogy and Petrology, 143(2), 209–218.
745 doi:10.1007/s00410-001-0320-y
746 Sourirajan, S., and Kennedy, G.C. (1962) The system H_2O-NaCl at elevated temperatures
747 and pressures. American Journal of Science, 260, 115–141.
748 Sowerby, J.R., and Keppler, H. (1999) Water speciation in rhyolitic melt determined by
749 in-situ infrared spectroscopy. American Mineralogist, 84, 1843-1849.
750 Spilliaert, N., Metrich, N., and Allard, P. (2006) S–Cl–F degassing pattern of water-rich
751 alkali basalt: Modelling and relationship with eruption styles on Mount Etna volcano.
752 Earth and Planetary Science Letters, 248(3-4), 772–786.
753 Stebbins, J.F. (1987) Identification of multiple structural species in silicate glasses by ^{29}Si
754 NMR. Nature, 330, 465–467.
755 Stebbins, J.F., and Du, L.-S. (2002) Chloride ion sites in silicate and aluminosilicate
756 glasses: A preliminary study by ^{35}Cl solid-state NMR. American Mineralogist, 87,
757 359–363.

758 Tamic, N., Behrens, H., and Holtz, F. (2001) The solubility of H_2O and CO_2 in rhyolitic
759 melts in equilibrium with a mixed CO_2-H_2O fluid phase. Chemical Geology, 174,
760 333–347.
761 Van Thiel, M., Becker, E.D., and Pimentel, G.C. (1957) Infrared studies of hydrogen
762 bonding of water by the matrix isolation technique. Journal of Chemical Physics, 27,
763 486–490.
764 Velde, B. (1983) Infrared OH stretch bands in potassic micas, talcs and saponites;
765 influence of electronic configuration and site of charge compensation. American
766 Mineralogist, 68, 1169–1173.
767 Walrafen, G.E. (1968) Raman Spectral Studies of HDO in H_2O. The Journal of Chemical
768 Physics, 48, 244.
769 Walrafen, G.E., Fisher, M.R., Hokmabadi, M.S., and Yang, W.H. (1986) Temperature
770 dependence of the low- and high-frequency Raman scattering from liquid water.
771 Journal of Chemical Physics, 85, 6970–6982.
772 Walfaren, G.E., Yang, W.H., Chu, Y.C., and Hokmabadi, M.S. (1996). Raman OD-
773 stretching overtone spectra from liquid D_2O between 22 and 152ºC, Journal of
774 Physical Chemistry, 100, 1381–1391.
775 Weber, C.F., Beahm, E.C., Lee, D.D., and Watson, J.S. (2000) A solubility model for
776 aqueous solutions containing sodium, fluoride, and phosphate ions. Industrial and
777 Engineering Chemistry Research, 39(2), 518-526.
778 Webster, J.D. (1992) Water solubility and chlorine partitioning in Cl-rich granitic
779 systems: Effects of melt composition at 2 kbar and 800ºC. Geochimica et
780 Cosmochimica Acta, 56, 679–687.

781 Webster, J.D. (1997) Exsolution of magmatic volatile phases from Cl-enriched
782 mineralizing granitic magmas and implications for ore metal transport. Geochimica
783 et Cosmochimica Acta, 61(5), 1017–1029.
784 Webster, J.D., Kinzler, R.J., and Mathez, E.A. (1999) Chloride and water solubility in
785 basalt and andesite melts and implications for magmatic degassing. Geochimica et
786 Cosmochimica Acta, 63(5), 729–738.
787 Williams T.J., Candela P.A., and Piccoli P.M. (1997) Hydrogen-alkali exchange between
788 silicate melts and two-phase aqueous mixtures: An experimental investigation.
789 Contributions to Mineralology and Petrology, 128, 114-126.
790 Withers, A.C., Zhang, Y., and Behrens, H. (1999). Reconciliation of experimental results
791 on H_2O speciation in rhyolitic glass using in-situ and quenching techniques. Earth
792 and Planetary Science Letters, 173(3), 343-349.
793 Yamamoto K., Nakanishi T., Kasahara H., and Abe K. (1983) Raman scattering of SiF4
794 molecules in amorphous fluorinated silicon., Journal of Non-Crystalline Solids, 59-
795 60, 213–216.
796 Zajacz, Z., Halter, W.E., Pettke, T., and Guillong, M. (2008) Determination of fluid/melt
797 partition coefficients by LA-ICPMS analysis of co-existing fluid and silicate melt
798 inclusions: Controls on element partitioning. Geochimica et Cosmochimica Acta,
799 72(8), 2169–2197. doi:10.1016/j.gca.2008.01.034
800 Zimova, M., and Webb, S.L. (2006) The effect of chlorine on the viscosity of Na_2O-
801 Fe_2O_3-Al_2O_3-SiO_2 melts. American Mineralogist, 91(2-3), 344–352.

802 Zotov, N., and Keppler, H. (1998) The structure of sodium tetrasilicate glass from
803 neutron diffraction, reverse Monte Carlo simulations and Raman spectroscopy.
804 Physics and Chemistry of Minerals 25(4), 259-267.
805 Zotov, N., and Keppler, H. (2000) In-situ Raman spectra of dissolved silica species in
806 aqueous fluids to 900ºC and 14 kbar. American Mineralogist, 85, 600–604.
807 Zotov, N., and Keppler, H. (2002) Silica speciation in aqueous fluids at high pressures
808 and high temperatures. Chemical Geology, 184, 71–82.
809
810
811
812

FIGURE CAPTIONS

Figure 1: Photomicrographs of the sample chamber in the HDAC at ambient temperature and 1 atm pressure. Starting materials include a grain of NS3A5 glass, a 0.5M NaF aqueous fluid and a ^{13}C diamond chip.

Figure 2: Photomicrographs of the sample in Fig. 1, before the heating process noted initial state (1), after heating process at 800ºC (2) and during cooling stages to ambient conditions (3 to 6).

Figure 3: A. Example of Raman spectrum of ^{13}C diamond inside the HDAC at ambient temperature and pressure conditions (solid line), at 400ºC and 358 MPa (dashed line) and at 800ºC and 1264 MPa (dotted line), as indicated. The peak marked "natural diamond" is the peak of ^{12}C from the diamond of the diamond cell itself. The Neon reference line is also shown here. B. Pressure-temperature relationships among our experiments: diamonds are for the experiment without halogens, the crosses are for the experiment with the addition of NaF and the circles are for the experiment with the addition of NaCl. Pressure-temperature relationships in aluminum-free $Na_2O.4SiO_2$ (NS4) and with 10mol% Al (NS4A10) (Mysen, 2010; 2011) are also shown.

Figure 4: Example of Raman spectra collected at high temperature and pressure in F-bearing melts and fluids. The frequency range highlighted in grey (A) refers to the second-order vibrations of the diamond anvils. The intensity of peaks shown in B and C

836 changes with *P-T* conditions and with the presence of either F or Cl in both melt and
837 fluid.
838
839 **Figure 5:** A. FTIR spectrum of a Cl-bearing H_2O-rich melt at 700 ºC in the 4200-5600
840 cm^{-1} region. B. Relationship between the ratio of integrated areas, A_{4500}/A_{5200}, vs.
841 temperature, for F-bearing (crosses) and Cl-bearing (circles) H_2O-rich melts.
842 Experimental data are compared with HDAC studies of halogen-free water-saturated
843 Na_2Si_4O9 (NS4) and $Na_2AlSi_3O_9$ (NA10) melts (Mysen 2009, 2011). Melt spectra were
844 obtained at different pressures up to: 1033 MPa for NS4, 791 MPa for NA10, 606 MPa
845 for F-bearing experiment and 1264 MPa for Cl-bearing experiment (Fig. 3b).
846
847 **Figure 6:** Raman spectra used to describe the extent of hydrogen bonding in H_2O-rich
848 NS3A5 melt and aqueous fluid. A. Example of a curve-fitted Raman spectrum in the
849 frequency range 3000-4000 cm^{-1} of a silicate-rich fluid recorded in-situ at elevated
850 temperature and pressure. Modified Van't Hoff expression of ln K vs. 1/T were employed
851 to calculate the stability hydrogen bonding in coexisting water-saturated aluminosilicate
852 melt (full symbols) and silicate-saturated aqueous fluid (empty symbols), for the halogen-
853 free experiment, B; the F-bearing experiment, C; and the Cl-bearing experiment, D. Note
854 that ΔH-values are derived from the lnK vs. 1/T slope with no correction for pressure.
855
856 **Figure 7:** Examples of Raman spectra in the frequency range of first-order (Si,Al)-O
857 vibrations from the halogen-free H_2O-rich melt (A); the F-bearing hydrous (B), and the
858 Cl-bearing fluid (C), at the pressure-temperature conditions indicated on individual

spectra. Grey lines are the Raman spectra and the black lines are the result of the curve fitting. Spectra are normalized to 100% intensity, where 100% represents the highest intensity of each spectrum. Residues of the curve-fittings are also presented.

Figure 8: Partition coefficients between fluid and melt, $D^{fluid/melt}$, for Q^0, Q^1, Q^2, and Q^3 species as a function of temperature. The $D^{fluid/melt}$ were calculated from each Q^n specie area normalized to the sum of all Q^n areas. Diamonds are data from the halogen-free experiment, crosses from the F-bearing experiment and circles from the Cl-bearing experiment.

Figure 9: Partition coefficients of Si-F between fluid and melt, $D^{fluid/melt}$ as a function of temperature (A); $\ln D^{fluid/melt}$ as function of $1/T.10^3$ (B), $\ln D_{Q3}{}^{fluid/melt}$ as function of $1/T.10^3$ in NS3A5 + H_2O + NaF experiment (C) and integrated Si-F band area of F-bearing melts (D). The $D^{fluid/melt}$ and the $Si\text{-}F_{melt}$ were calculated from the 990 cm^{-1} band area normalized to the sum of all Q^n integrated peak areas.

889 **TABLES**
890
891
892 Table 1. Run data
893

Temp (ºC)	Raman shift ^{13}C diamond (cm^{-1})	[a]Pressure ^{13}C diamond (MPa)	Phase present
		Experiment NS3A5 + pure H_2O fluid	
		T_h = 210ºC- Fluid density = 0.853 g.cm^{-3}	
800	1264.6	829	Melt (R[b]), Fluid (R),^{13}C
700	1268.7	710	Melt (R), Fluid (R),^{13}C
600	1271.6	575	Melt (R), Fluid (R),^{13}C
500	1274	423	Melt (R), Fluid (R),^{13}C
400	1276.1	255	Quartz, Melt (R), Fluid (R),^{13}C
300	1278.2	143	Quartz, Melt (R), Fluid (R),^{13}C
		Experiment NS3A5 + H_2O + 0.5M NaF fluid	
		T_h = 340ºC- Fluid density = 0.611 g.cm^{-3}	
800	1264	606	Melt (R, IR[b]), Fluid (R, IR),^{13}C
700	1264	448	Melt (R, IR), Fluid (R, IR),^{13}C
600	1268	365	Melt (R, IR), Fluid (R, IR),^{13}C
500	1271.8	313	Salt[c], Melt (R, IR), Fluid (R, IR),^{13}C
400	1274.4	218	Salt, Melt (R, IR), Fluid (R, IR),^{13}C
300	1277.2	143	Salt, Melt (R, IR), Fluid (R, IR),^{13}C
		Experiment NS3A5 + H_2O + 0.5M NaCl fluid	
		T_h = 340ºC- Fluid density = 0.926 g.cm^{-3}	
800	1266	1264	Melt (R), Fluid (R),^{13}C
780	1266.3	1237	Melt (R), Fluid (R),^{13}C
720			Melt (IR), Fluid (IR)
700	1268.7	1072	Melt (R, IR), Fluid (R, IR),^{13}C
600	1271.9	790	Melt (R, IR), Fluid (R, IR),^{13}C
500	1274.8	638	Salt, Melt (R, IR), Fluid (R, IR),^{13}C
400	1276.4	358	Salt, Melt (R, IR), Fluid (R, IR),^{13}C
300	1278.4	246	Salt, Melt (R, IR), Fluid (R, IR),^{13}C

894
895 [a] Pressure calculated from the ^{13}C diamond shift normalized to the 584.72 nm Ne line (see
896 text for further discussion).
897 [b] R – Raman spectra recorded. IR – infrared spectra recorded.
898 [c] Salt refers to salt precipitation.

This is a preprint, the final version is subject to change, of the American Mineralogist (MSA)
Cite as Authors (Year) Title. American Mineralogist, in press.
(DOI will not work until issue is live.) DOI: http://dx.doi.org/10.2138/am-2015-4859

899 Table 2. Silicate species, Q^n, abundance in melt and fluid of each experiment.
900

Temp (°C)	Q^0	Q^1	Q^2	Q^3	Q^3(F)
		Experiment NS3A5 + pure H_2O fluid			
		Melt			
700	0.127(3)	0.467(8)	0.246(7)	0.160(5)	
600	0.057(1)	0.224(4)	0.433(4)	0.286(4)	
500	0.039(1)	0.147(3)	0.455(5)	0.358(4)	
400	0.029(0.4)	0.209(3)	0.409(6)	0.351(6)	
		Fluid			
700	0.376(3)	0.277(2)	0.095(1)	0.251(2)	
600	0.399(4)	0.180(3)	0.095(1)	0.326(6)	
500	0.505(5)	0.107(1)	0.075(1)	0.313(3)	
400	0.563(2)	0.127(1)	0.069(2)	0.240(3)	
		Experiment NS3A5 + H_2O + 0.5M NaF fluid			
		Melt			
800	0.232(3)	0.326(4)	0.116(2)	0.238(4)	0.087(2)
700	0.191(5)	0.310(8)	0.121(4)	0.244(14)	0.134(4)
600	0.053(1)	0.218(3)	0.108(2)	0.398(6)	0.223(3)
500	0.026(1)	0.118(2)	0.111(2)	0.507(6)	0.237(3)
400	0.034(2)	0.083(3)	0.105(4)	0.521(11)	0.257(6)
		Fluid			
800	0.435(6)	0.139(2)	0.121(2)	0.176(3)	0.128(2)
700	0.450(6)	0.129(2)	0.181(3)	0.098(2)	0.142(2)
600	0.438(2)	0.106(2)	0.174(3)	0.107(2)	0.174(3)
500	0.516(7)	0.160(1)	0.160(1)	0.066(0.5)	0.099(1)
400	0.629(14)	0.150(5)	0.113(3)	0.052(2)	0.056(2)
		Experiment NS3A5 + H_2O + 0.5M NaCl fluid			
		Melt			
800	0.259(4)	0.289(5)	0.288(5)	0.163(4)	
780	0.196(2)	0.261(3)	0.404(5)	0.140(3)	
700	0.059(2)	0.339(5)	0.376(8)	0.226(3)	
600	0.045(1)	0.347(5)	0.342(8)	0.265(2)	
500	0.061(0.5)	0.314(4)	0.409(9)	0.215(3)	
400	0.047(1)	0.207(3)	0.610(11)	0.135(3)	
		Fluid			
800	0.432(4)	0.108(2)	0.179(3)	0.280(4)	
780	0.458(3)	0.094(1)	0.217(2)	0.230(2)	
700	0.564(6)	0.067(0.5)	0.154(1)	0.215(1)	
600	0.583(8)	0.064(1)	0.148(2)	0.204(3)	
500	0.621(7)	0.037(1)	0.135(2)	0.207(3)	
400	0.611(9)	0.045(1)	0.134(1)	0.209(3)	

901 Numbers in parentheses represents one standard deviation in terms of least units cited.

This is a preprint, the final version is subject to change, of the American Mineralogist (MSA)
Cite as Authors (Year) Title. American Mineralogist, in press.
(DOI will not work until issue is live.) DOI: http://dx.doi.org/10.2138/am-2015-4859

902 **FIGURES**
903
904
905 **Figure 1**
906
907

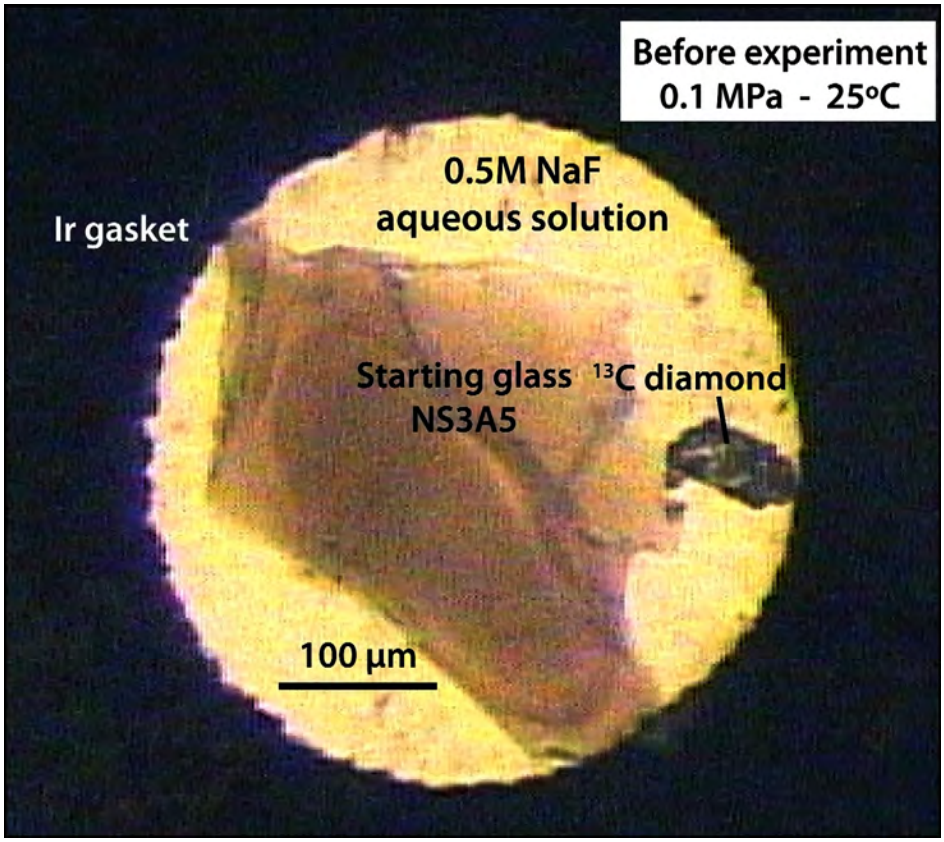

908
909
910
911
912
913
914
915
916
917
918
919
920
921
922
923
924

925 **Figure 2**
926
927

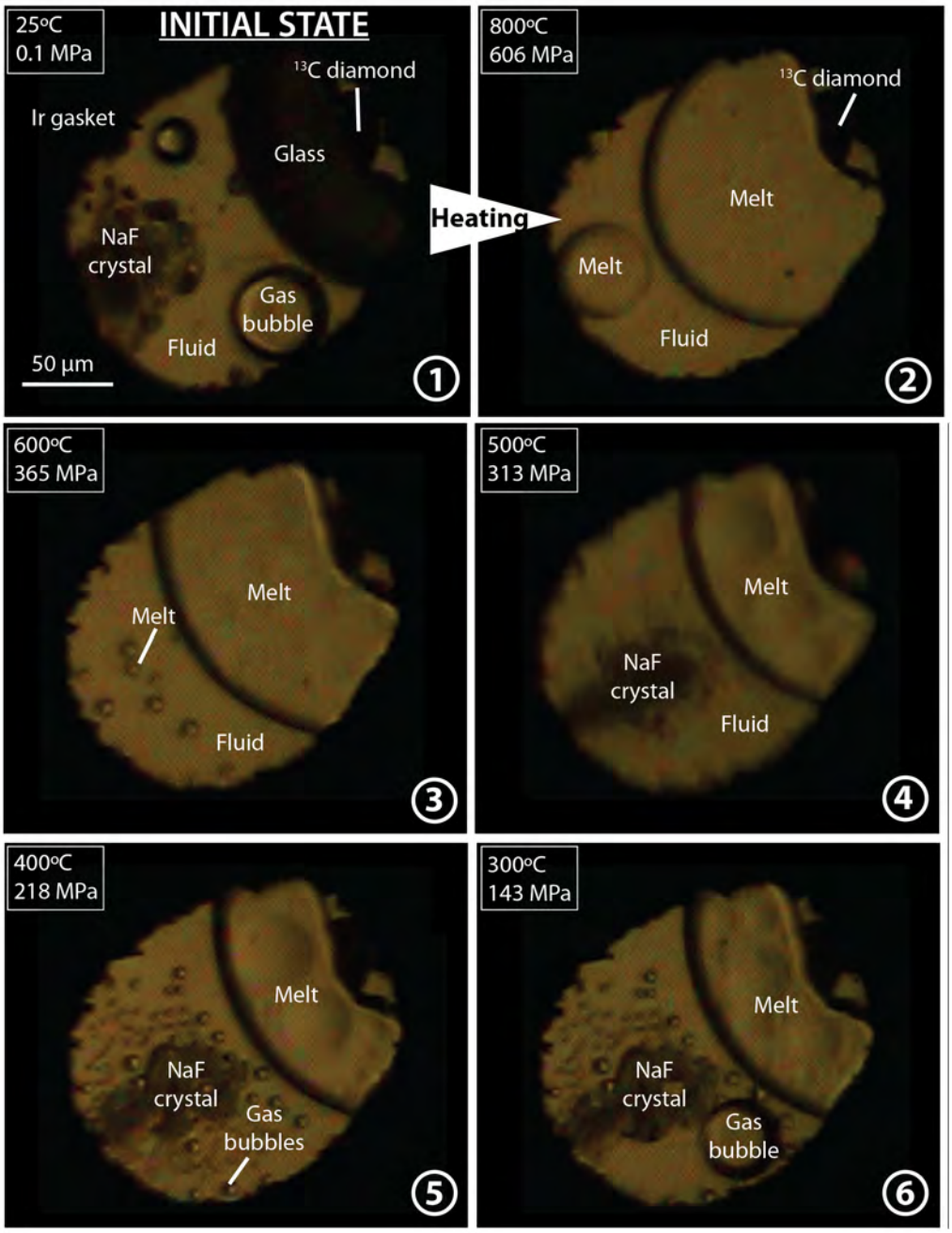

928
929
930
931

This is a preprint, the final version is subject to change, of the American Mineralogist (MSA)
Cite as Authors (Year) Title. American Mineralogist, in press.
(DOI will not work until issue is live.) DOI: http://dx.doi.org/10.2138/am-2015-4859

Figure 3

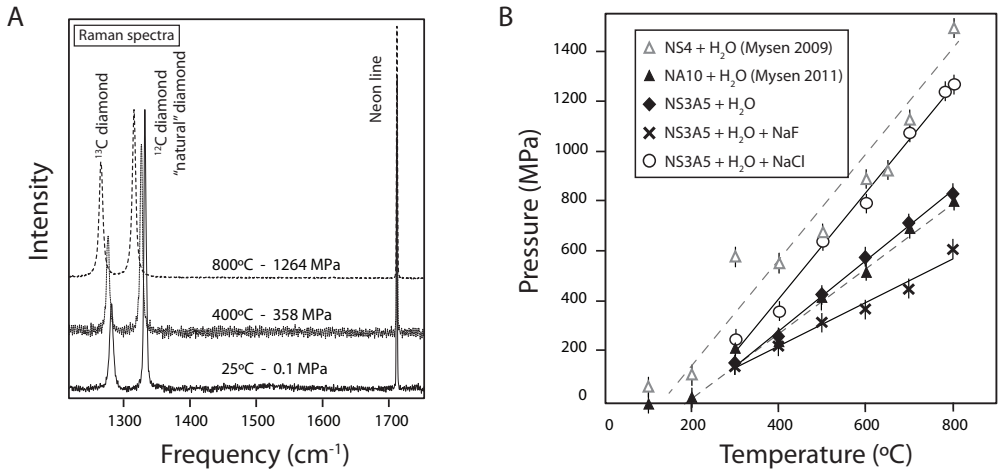

Figure 4

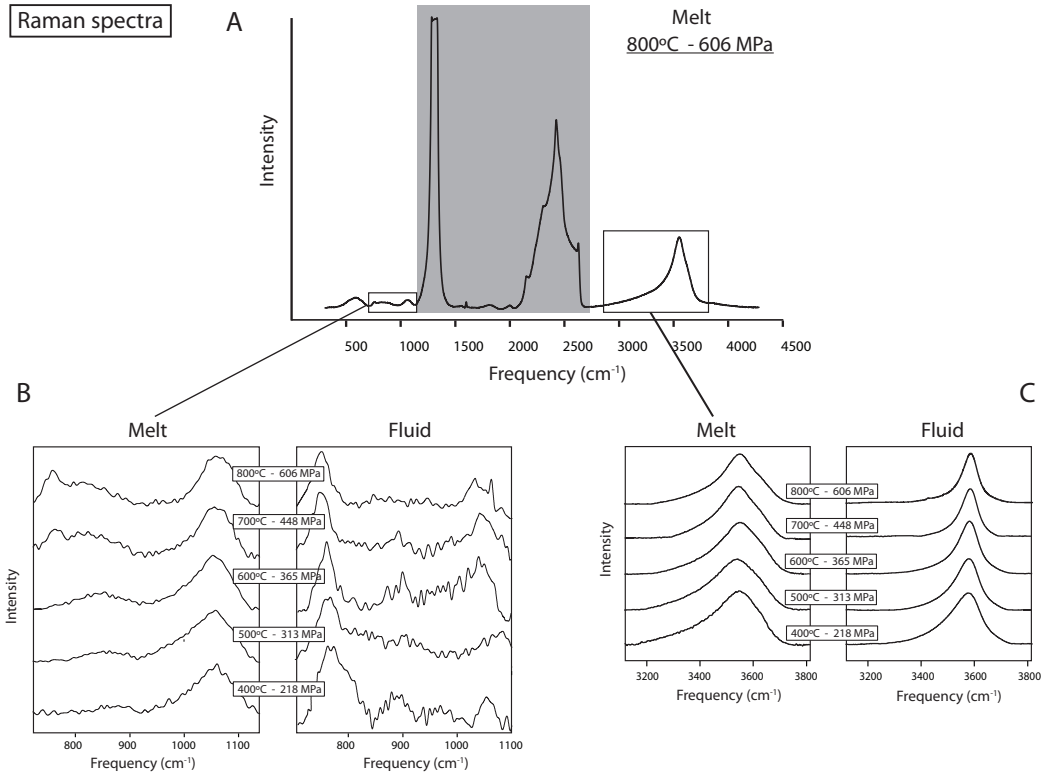

Figure 5

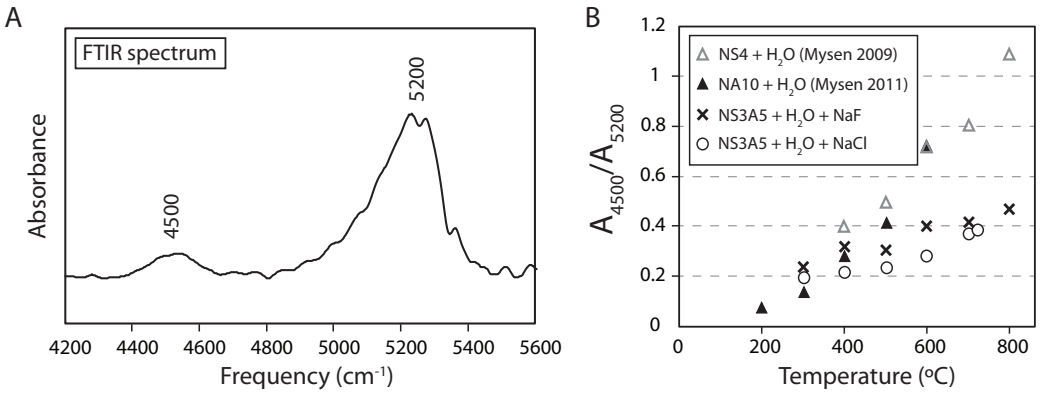

Figure 6

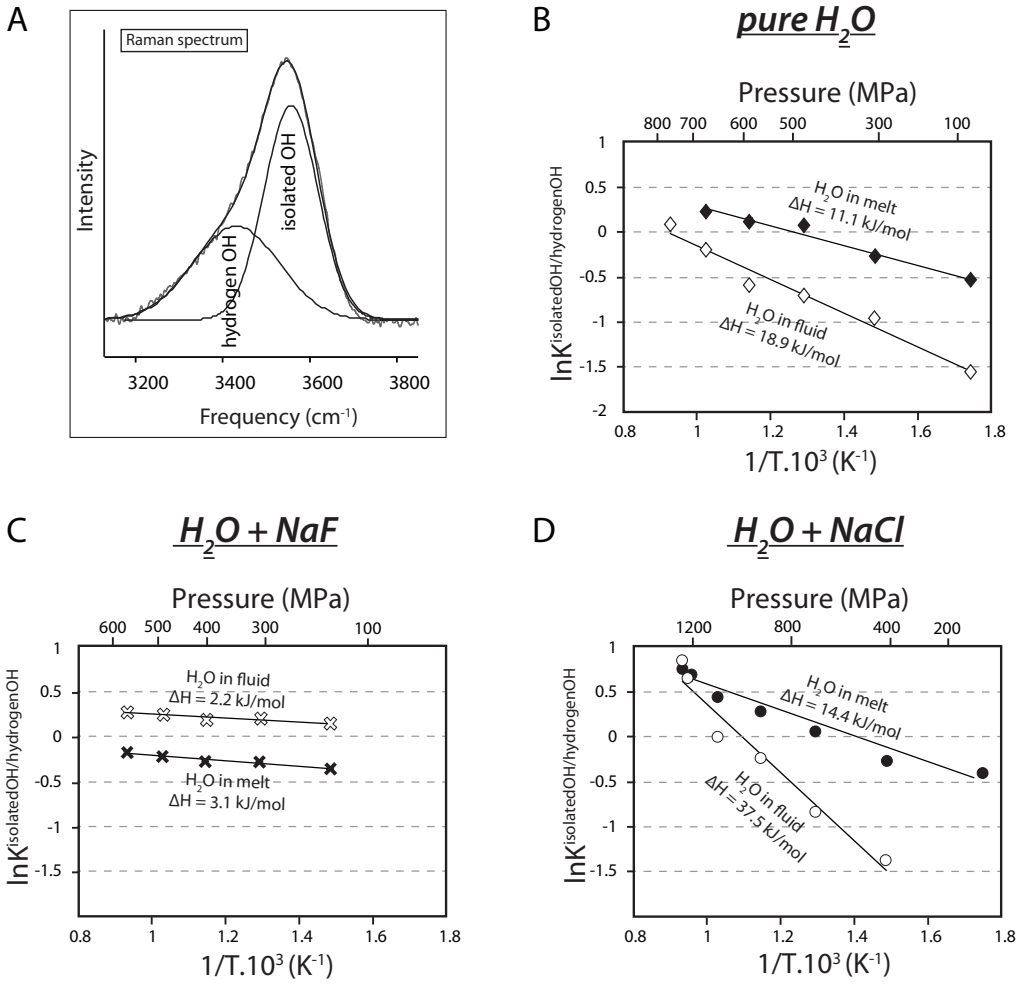

Figure 7

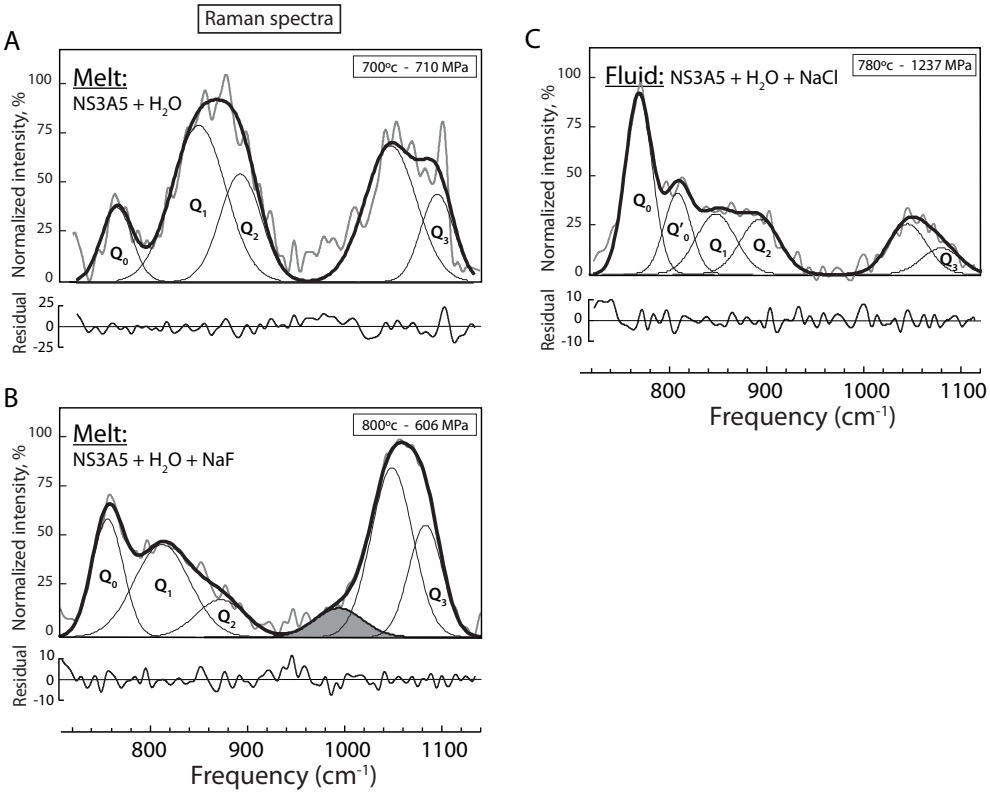

Figure 8

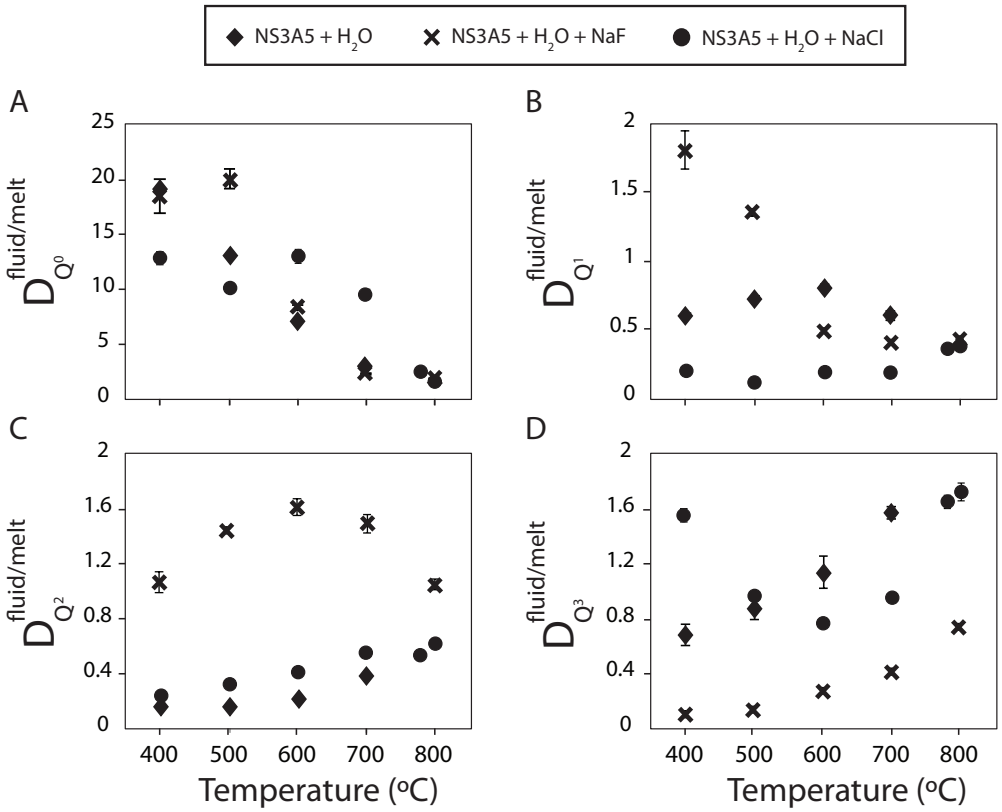

Figure 9